Correlations in the isotropic phases of chiral liquid crystals: The role of helicity modes

L. Longa,[1,2] M. Cieśla,[1] and H.-R. Trebin[2]
[1]*Marian Smoluchowski Institute of Physics, Department of Statistical Physics, Jagellonian University, Reymonta 4, Kraków, Poland*
[2]*Institut für Theoretische und Angewandte Physik, Universität Stuttgart, Pfaffenwaldring 57, D-70550 Stuttgart, Germany*
(Received 10 January 2003; published 20 June 2003)

The phenomenological theory of chiral liquid crystals is further developed by generalizing the model of self-consistent correlations [J. Englert, L. Longa, H. Stark, and H.-R. Trebin, Phys. Rev. Lett. **81**, 1457 (1998)]. In the present approach, not only a leading helicity mode of the tensor order parameter is retained but also the remaining four modes. By considering a full fluctuating spectrum of the order parameter, the role of correlations between helicity modes in the isotropic phases is studied. Additionally, an exact form of the two-point correlation function in real space is derived and its properties are thoroughly discussed. It is shown that for chiral isotropic liquids purely chiral modes could be identified that do not exist for an ordinary liquid. Detailed results of the numerical calculations are compared with those obtained from the earlier model and these show regions where the coupling between the modes becomes important, in agreement with the available experimental data. Though the analysis up to first-order cumulant expansion does not predict a direct phase transition between the blue phase III and the isotropic phase, it is fairly easy to identify two differently correlated regions in a temperature-chirality plane. Various structural quantities, such as optical activity and specific heat, also reveal a behavior characteristic of two isotropic phases with different correlation lengths.

DOI: 10.1103/PhysRevE.67.061705 PACS number(s): 61.30.−v, 64.70.−p, 05.40.−a, 61.20.−p

I. INTRODUCTION

In our previous publications [1,2], we have demonstrated that correlations between orientational degrees of freedom are crucial for a proper understanding of phase diagrams, involving isotropic, cholesteric, and cubic blue phases. In particular, we showed that it is possible to construct a systematic perturbational scheme to account for the complexity of the phase diagram for blue phases. In the previous analysis, however, we neglected the coupling between the modes of the tensor order parameter. Only the leading order calculations, including the $m=2$ helicity mode of the tensor order parameter, have been carried out.

On the other hand, experiments show that other helicity modes and coupling between them may become important in the pretransitional regime [3–7]. For example, light scattering in the isotropic phase gives a possibility to observe all five helicity modes. There are also correlations between the modes as probed, e.g., by optical activity experiments.

In the present approach, we systematically include *all five helicity modes* into a field theoretical treatment of the isotropic phases with Landau–de Gennes Hamiltonian. We also study the coupling between the modes and show explicitly the existence of this coupling in the pretransitional regime, at theoretical level. In addition, our analysis also provides a simple measure of chirality in the isotropic phase, in terms of invariant tensors extracted from real-space correlation functions. A semiphenomenological approach to this problem, valid in the vicinity of the isotropic–blue phase III (BP III) phase transition, has been proposed in the literature [8].

This paper is organized as follows. After a brief discussion of the statistical field theory, we derive an exact representation of pair correlations in the isotropic phase and discuss a possible relation to phase chirality. Then, we describe a general perturbation scheme based on an effective Hamiltonian, which depends on five variational parameters. These play the role of the inverse square roots of the correlation lengths for the alignment tensor field. Using a cumulant expansion and variational calculus, we explicitly show that the five modes are not only visible in the pretransitional region but also are strongly coupled. Our cumulant expansion is limited to leading order as previously. A third-order expansion with the exact Hamiltonian is still extremely complicated and demanding and is reserved for future work. In the last section, we apply the theory to calculate observables such as the rotatory power.

II. THEORY OF ORIENTATIONAL ORDER IN CHOLESTERIC LIQUID CRYSTALS

An average orientational order in liquid crystals is best quantified in terms of the symmetric and traceless alignment tensor field $\boldsymbol{Q}(\boldsymbol{r})$. The Landau–Ginzburg–de Gennes Hamiltonian, also known as free energy functional of chiral liquid crystals, follows then from a series expansion in $\boldsymbol{Q}(\boldsymbol{r})$ and its derivatives. In real space, it reads [9]

$$H=H_2+H_3+H_4, \tag{1}$$

where

$$H_2=\frac{1}{2}\int_V d^3\boldsymbol{r}[a\,\mathrm{Tr}(\boldsymbol{Q}^2)+c_1Q_{ij,l}Q_{ij,l}+c_2Q_{ij,i}Q_{lj,l} -2d\epsilon_{ijl}Q_{in}Q_{ln,j}], \tag{2}$$

$$H_3=-\frac{\beta}{\sqrt{24}}\int_V d^3\boldsymbol{r}\,\mathrm{Tr}(\boldsymbol{Q}^3), \quad H_4=\frac{\gamma}{24}\int_V d^3\boldsymbol{r}[\mathrm{Tr}(\boldsymbol{Q}^2)]^2. \tag{3}$$

The stability of the expansion (1) requires that $c_2 > -\frac{3}{2}c_1$ and $\gamma > 0$. Additionally, as usual in Landau theory, the parameter a is the temperature distance from the spinodal, $a = a_0(T - T^*)$ with $a_0 > 0$.

The impact of the fluctuations of orientational degrees of freedom can now be analyzed with the formalism of statistical field theory. For example, the free energy and the ordinary two-point correlation function are given by

$$F = -k_B T \ln Z, \quad Z = \int D\boldsymbol{Q} \exp(-H/k_B T), \tag{4}$$

$$\begin{aligned}\tilde{G}_{\alpha\beta\gamma\delta}(\boldsymbol{r},\boldsymbol{r}') &= \langle Q_{\alpha\beta}(\boldsymbol{r}) Q_{\gamma\delta}(\boldsymbol{r}')\rangle \\ &= Z^{-1} \int D\boldsymbol{Q} Q_{\alpha\beta}(\boldsymbol{r}) Q_{\gamma\delta}(\boldsymbol{r}') \exp(-H/k_B T),\end{aligned} \tag{5}$$

where the symbol $\int D\boldsymbol{Q}$ denotes the integral over the tensor field $\boldsymbol{Q}$. Note that $\tilde{G}_{\alpha\beta\gamma\delta}(\boldsymbol{r},\boldsymbol{r}')$ is a component of the fourth-rank $3\times3\times3\times3$ tensor $\tilde{\boldsymbol{G}} = \langle \boldsymbol{Q}(\boldsymbol{r}) \otimes \boldsymbol{Q}(\boldsymbol{r}')\rangle$.

Practical calculations involving Eqs. (4) and (5) are carried out in the momentum representation as it diagonalizes H_2. It amounts to expanding $\boldsymbol{Q}(\boldsymbol{r})$ into a Fourier series and spin tensor modes of momentum $L = 2$, and yields

$$\boldsymbol{Q}(\boldsymbol{r}) = \sum_{\tilde{\boldsymbol{k}}} \sum_{m=-2}^{2} Q_m(\tilde{\boldsymbol{k}}) \boldsymbol{M}_m(\hat{\boldsymbol{k}}) e^{i\tilde{\boldsymbol{k}}\cdot\boldsymbol{r}}. \tag{6}$$

The basis matrices $\boldsymbol{M}_m(\hat{\boldsymbol{k}})$ are defined separately for each wave vector direction $\hat{\boldsymbol{k}}$ and m labels the different helicity modes. In a right-handed local system of orthonormal unit vectors $\{\hat{\boldsymbol{\xi}}, \hat{\boldsymbol{\eta}}, \hat{\mathbf{k}} = \tilde{\mathbf{k}}/\tilde{k}\}$, the basis matrices read

$$\boldsymbol{M}_0(\hat{\boldsymbol{k}}) = \frac{1}{\sqrt{6}}(3\hat{\mathbf{k}}\otimes\hat{\mathbf{k}} - \mathbf{1}),$$

$$\begin{aligned}\boldsymbol{M}_1(\hat{\boldsymbol{k}}) &= \frac{1}{\sqrt{2}}(\boldsymbol{u}\otimes\hat{\boldsymbol{k}} + \hat{\boldsymbol{k}}\otimes\boldsymbol{u}) = [\boldsymbol{M}_{-1}(\hat{\boldsymbol{k}})]^*, \\ \boldsymbol{M}_2(\hat{\boldsymbol{k}}) &= \boldsymbol{u}\otimes\boldsymbol{u}, = [\boldsymbol{M}_{-2}(\hat{\boldsymbol{k}})]^*,\end{aligned} \tag{7}$$

where $\boldsymbol{u} = 1/\sqrt{2}(\hat{\boldsymbol{\xi}} + \mathrm{i}\hat{\boldsymbol{\eta}})$, $\tilde{k} = |\tilde{\mathbf{k}}|$, and

$$\boldsymbol{M}_m(\hat{\boldsymbol{k}}) \cdot \boldsymbol{M}^*_{m'}(\hat{\boldsymbol{k}}) \equiv \mathrm{Tr}[\boldsymbol{M}_m(\hat{\boldsymbol{k}}) \boldsymbol{M}^*_{m'}(\hat{\boldsymbol{k}})] = \delta_{mm'}. \tag{8}$$

In the reciprocal space and in the dimensionless variables of Grebel *et al.* [9],

$$\begin{aligned}&\boldsymbol{x} = \boldsymbol{r}/\xi_R, \quad \boldsymbol{k} = \tilde{\boldsymbol{k}}\xi_R, \quad v = V/\xi_R^3, \\ &\mu_m(\boldsymbol{k}) = Q_m(\boldsymbol{k})/s, \quad H = \gamma s^4 \mathcal{H}, \\ &s = \beta/\sqrt{6}\gamma, \quad \kappa = \xi_R d/c_1, \quad \rho = c_2/c_1 > -\frac{3}{2}, \quad \mathcal{T} = k_B T \gamma s^4, \\ &t = 2a/\gamma s^2 = a_0(\mathcal{T} - \mathcal{T}_0)/\mathcal{T}_0, \quad a_0 > 0, \quad \xi_R = \sqrt{2c_1/\gamma s^2},\end{aligned} \tag{9}$$

the Hamiltonian (1) becomes [1,2]

$$\begin{aligned}\mathcal{H}/v = &\frac{1}{4}\sum_{\boldsymbol{k}}\sum_{m}\left\{t - m\kappa k + \left[1 + \frac{1}{6}\rho(4-m^2)\right]k^2\right\}|\mu_m(k)|^2 - \frac{1}{2}\sum_{\boldsymbol{k}_1,\boldsymbol{k}_2,\boldsymbol{k}_3}\sum_{m_1,m_2,m_3}\mathrm{Tr}[\boldsymbol{M}_{m_1}(\hat{\boldsymbol{k}}_1)\boldsymbol{M}_{m_2}(\hat{\boldsymbol{k}}_2)\boldsymbol{M}_{m_3}(\hat{\boldsymbol{k}}_3)] \\ &\times \mu_{m_1}(\boldsymbol{k}_1)\mu_{m_2}(\boldsymbol{k}_2)\mu_{m_3}(\boldsymbol{k}_3)\delta_{\boldsymbol{k}_1+\boldsymbol{k}_2+\boldsymbol{k}_3,\boldsymbol{0}} + \frac{1}{24}\sum_{\boldsymbol{k}_1,\boldsymbol{k}_2,\boldsymbol{k}_3,\boldsymbol{k}_4}\sum_{m_1,m_2,m_3,m_4}\mathrm{Tr}[\boldsymbol{M}_{m_1}(\hat{\boldsymbol{k}}_1)\boldsymbol{M}_{m_2}(\hat{\boldsymbol{k}}_2)]\mathrm{Tr}[\boldsymbol{M}_{m_3}(\hat{\boldsymbol{k}}_3)\boldsymbol{M}_{m_4}(\hat{\boldsymbol{k}}_4)] \\ &\times \mu_{m_1}(\boldsymbol{k}_1)\mu_{m_2}(\boldsymbol{k}_2)\mu_{m_3}(\boldsymbol{k}_3)\mu_{m_4}(\boldsymbol{k}_4)\delta_{\boldsymbol{k}_1+\boldsymbol{k}_2+\boldsymbol{k}_3+\boldsymbol{k}_4,\boldsymbol{0}}.\end{aligned} \tag{10}$$

In deriving Eq. (10), use has been made of the normalization $1/v\int_v e^{i\boldsymbol{k}\cdot\boldsymbol{x}} d^3\boldsymbol{x} = \delta_{\boldsymbol{k},\boldsymbol{0}}$ and of the reality condition $\mu_m(-\boldsymbol{k}) = (-1)^m \mu^*_m(\boldsymbol{k})$ for the field $\boldsymbol{Q}(\boldsymbol{r})$. For the transformed Hamiltonian, Eqs. (4) and (5) read

$$Z = \int D\boldsymbol{\mu} \exp(-\mathcal{H}/\mathcal{T}), \tag{11}$$

and the dimensionless correlation function is given by

$$\begin{aligned}\boldsymbol{G}(\boldsymbol{x},\boldsymbol{x}') &= s^{-2}\tilde{\boldsymbol{G}}(\boldsymbol{x},\boldsymbol{x}') \\ &= \sum_{\substack{\boldsymbol{k}_1,m_1 \\ k_1<\Lambda}}\sum_{\substack{\boldsymbol{k}_2,m_2 \\ k_2<\Lambda}} \boldsymbol{M}_{m_1}(\hat{\boldsymbol{k}}_1)\otimes\boldsymbol{M}_{m_2}(\hat{\boldsymbol{k}}_2)\, e^{i(\boldsymbol{k}_1\cdot\boldsymbol{x}+\boldsymbol{k}_2\cdot\boldsymbol{x}')} \\ &\quad\times\langle \mu_{m_1}(\boldsymbol{k}_1)\mu_{m_2}(\boldsymbol{k}_2)\rangle,\end{aligned} \tag{12}$$

where

$$\langle \mu_{m_1}(\boldsymbol{k}_1)\mu_{m_2}(\boldsymbol{k}_2)\rangle = Z^{-1}\int D\boldsymbol{\mu}\mu_{m_1}(\boldsymbol{k}_1)\mu_{m_2}(\boldsymbol{k}_2) \times \exp(-\mathcal{H}/\mathcal{T}). \quad (13)$$

Λ is the dimensionless cutoff and $D\boldsymbol{\mu} = \Pi_{k<\Lambda}^{m,\boldsymbol{k}}[\sqrt{v/2\pi}d\mu_m(\boldsymbol{k})]$. The moduli of all wave vectors entering sums in the Eq. (10) do not exceed Λ.

III. GENERAL ANALYSIS OF THE REAL-SPACE TWO-POINT CORRELATION FUNCTIONS IN THE ISOTROPIC PHASE

In this section, we define correlation functions that we are going to calculate for chiral isotropic liquids. We restrict ourselves to the most important and the simplest of correlation functions, namely, to the two-point correlation function $\boldsymbol{G}(\boldsymbol{x},\boldsymbol{x}')$. It describes processes taking place in isotropic as well as in anisotropic liquids that are related to fluctuations in the alignment tensor. Leading terms of the light scattering amplitude as well as of the optical activity of chiral liquid crystals serve here as examples. Moreover, invariant tensors extracted from $\boldsymbol{G}$ can be used to define phase chirality, where the latter issue is being widely discussed recently in the literature [6,10,11]. Knowing real-space properties of $\boldsymbol{G}(\boldsymbol{x},\boldsymbol{x}')$ would allow for comparison (and perhaps for finding a bridge) between computer simulations on model chiral liquid crystals (e.g., simulations of Memmer [11]) and the phenomenological theory. Below, we shall give an explicit formula for this correlation function in the isotropic liquid, in terms of its fourier modes, and show that these can be expressed as an integral over k involving products of five elementary correlation functions $\langle|\mu_m(\boldsymbol{k})|^2\rangle$ with terms such as $c_n=\cos(k|\boldsymbol{r}-\boldsymbol{r}'|)/(k|\boldsymbol{r}-\boldsymbol{r}'|)^n$ and $s_n=\sin(k|\boldsymbol{r}-\boldsymbol{r}'|)/(k|\boldsymbol{r}-\boldsymbol{r}'|)^n$.

For an isotropic fluid, $\boldsymbol{G}$ is invariant with respect to a global translation and a rotation about $\boldsymbol{x}-\boldsymbol{x}'$. These symmetry requirements reduce Eq. (12) to a simpler one, which reads

$$\boldsymbol{G}(\boldsymbol{x},\boldsymbol{x}') = \boldsymbol{G}(\boldsymbol{x}-\boldsymbol{x}') = \frac{v}{(2\pi)^2}\sum_m \int_0^\Lambda k^2 G_m(k)\boldsymbol{\mathcal{M}}_m(k|\boldsymbol{x}-\boldsymbol{x}'|,\hat{\boldsymbol{z}})dk \quad (14)$$

with

$$G_m(k) = \langle|\mu_m(\boldsymbol{k})|^2\rangle \quad (15)$$

and

$$\boldsymbol{\mathcal{M}}_m(k|\boldsymbol{x}-\boldsymbol{x}'|,\hat{\boldsymbol{z}}) = \frac{1}{4\pi}\int d^2\hat{\boldsymbol{k}}[\boldsymbol{M}_m(\hat{\boldsymbol{k}})\otimes\boldsymbol{M}_m^*(\hat{\boldsymbol{k}})]e^{ik|\boldsymbol{x}-\boldsymbol{x}'|\hat{\boldsymbol{k}}\cdot\hat{\boldsymbol{z}}}, \quad (16)$$

where $\hat{\boldsymbol{z}}=(\boldsymbol{x}-\boldsymbol{x}')/|\boldsymbol{x}-\boldsymbol{x}'|$. While general formula (14) depends on details of the five elementary correlations $G_m(k)$, the angular integrals (16) can be carried out explicitly. An average over the unit sphere of the fourth-rank tensor $[\boldsymbol{M}_m(\hat{\boldsymbol{k}})\otimes\boldsymbol{M}_m^*(\hat{\boldsymbol{k}})]$ with a function depending on $\hat{\boldsymbol{k}}\cdot\hat{\boldsymbol{z}}$ yields a uniaxial tensor. This, in turn, is decomposed with respect to a basis of fourth-rank uniaxial tensors

$$\boldsymbol{M}_0^{(L)} = \sum_{m_1,m_2}\begin{pmatrix} 2 & 2 & | & L \\ m_1 & m_2 & | & 0\end{pmatrix}\boldsymbol{M}_{m_1}(\hat{\boldsymbol{z}})\otimes\boldsymbol{M}_{m_2}(\hat{\boldsymbol{z}}). \quad (17)$$

Here $\{\hat{\boldsymbol{x}},\hat{\boldsymbol{y}},\hat{\boldsymbol{z}}=(\boldsymbol{x}-\boldsymbol{x}')/|\boldsymbol{x}-\boldsymbol{x}'|\}$ is the local, orthonormal tripod of vectors and

$$\begin{pmatrix} 2 & 2 & | & L \\ m_1 & m_2 & | & 0\end{pmatrix}$$

are Clebsch-Gordan coefficients. There are five such tensors, corresponding to $L=0,1,2,3,4$, which we present in the Appendix [Eqs. (A1)–(A5)]. Under rotations, these transform as spherical harmonics $Y_0^{(L)}$, and these are orthonormal:

$$\boldsymbol{M}_0^{(L)*}\cdot\boldsymbol{M}_0^{(L')} \equiv \sum_{\alpha\beta\gamma\delta}(\boldsymbol{M}_0^{(L)})^*_{\alpha\beta\gamma\delta}(\boldsymbol{M}_0^{(L')})_{\alpha\beta\gamma\delta} = \delta_{LL'}. \quad (18)$$

The integration in Eq. (16) is performed using the quaternion parametrization of the tripod $\{\hat{\boldsymbol{\xi}},\hat{\boldsymbol{\eta}},\hat{\boldsymbol{k}}\}$. Alternatively, one can perform a Legendre polynomial expansion of the exponential function in Eq. (16) and carry out integration by parts. With both methods, the final result for the real-space correlation function (14) reads

$$\boldsymbol{G}(\boldsymbol{x}-\boldsymbol{x}') = \frac{v}{(2\pi)^2}\sum_{L=0}^{4} G^{(L)}(|\boldsymbol{x}-\boldsymbol{x}'|)\boldsymbol{M}_0^{(L)}(\hat{\boldsymbol{z}}), \quad (19)$$

where

$$G^{(0)} = \frac{1}{\sqrt{5}}\left\langle\!\!\left\langle\left(\sum_{m=-2}^{2} G_m\right)u_0\right\rangle\!\!\right\rangle, \quad (20)$$

$$G^{(1)} = i\,G_R^{(1)} = \frac{i}{\sqrt{10}}\langle\!\langle(2\,G_{-2}-2\,G_2+G_{-1}-G_1)\,u_1\rangle\!\rangle, \quad (21)$$

$$G^{(2)} = \frac{1}{\sqrt{14}}\langle\!\langle(2\,G_{-2}+2\,G_2-2\,G_0-G_1-G_{-1})\,u_2\rangle\!\rangle, \quad (22)$$

$$G^{(3)} = i\,G_R^{(3)} = \frac{i}{\sqrt{10}}\langle\!\langle(G_{-2}-G_2+2\,G_1-2\,G_{-1})\,u_3\rangle\!\rangle, \quad (23)$$

$$G^{(4)} = \frac{1}{\sqrt{70}}\langle\!\langle(G_{-2}+G_2+6\,G_0-4\,G_1-4\,G_{-1})u_4\rangle\!\rangle, \quad (24)$$

with

$$u_0 = s_1, \quad u_1 = -iP_1\left(i\frac{\partial}{\partial(kr)}\right)s_1 = c_1 - s_2,$$

$$u_2 = P_2\left(i\frac{\partial}{\partial(kr)}\right)s_1 = 3c_2 + s_1 - 3\,s_3, \tag{25}$$

$$u_3 = -iP_3\left(i\frac{\partial}{\partial(kr)}\right)s_1 = c_1 - 15\,c_3 - 6\,s_2 + 15\,s_4, \tag{26}$$

$$u_4 = P_4\left(i\frac{\partial}{\partial(kr)}\right)s_1 = 10\,c_2 - 105\,c_4 + s_1 - 45\,s_3 + 105\,s_5, \tag{27}$$

$$\langle\langle G_m\, u_n\rangle\rangle = \int_0^\Lambda k^2 G_m(k)\, u_n(k|\boldsymbol{x}-\boldsymbol{x}'|)\,d\,k. \tag{28}$$

P_Ls are Legendre polynomials. Note that, in reciprocal as well as in real space there are only five different correlation functions (modes). In reciprocal space, these are the $G_m(k)$ functions while their counterparts in the real space are $G^{(L)}$, Eqs. (20)–(24),

$$G^{(L)} = \frac{(2\pi)^2}{v}\boldsymbol{G}(\boldsymbol{x}-\boldsymbol{x}')\cdot\boldsymbol{M}_0^{(L)*}. \tag{29}$$

The correlation functions in real space provide an elegant classification of the modes, which are read off from the formulas (21)–(24). In particular, we find that the modes $G^{(1)}$ and $G^{(3)}$ associated with the axial tensors $\boldsymbol{M}_0^{(1)}$ and $\boldsymbol{M}_0^{(3)}$, respectively, exist *only* for chiral systems, and disappear for racemic mixtures. These show that chirality locally induces polar correlations ($G^{(1)}$), even in the absence of the dipole moments. As follows from numerical analysis presented in the following section, the leading correlations in the isotropic, chiral liquid are given by $G^{(0)}$, $G^{(2)}$, and $G^{(1)}$, while $G^{(3)}$ and $G^{(4)}$ are less important. In the limit of $\boldsymbol{x}'\to\boldsymbol{x}$ and for fixed Λ, all correlations vanish except $G^{(0)}$, which is given by

$$G^{(0)}(0) = \frac{1}{\sqrt{5}}\left\langle\!\!\left\langle\left(\sum_{m=-2}^{2} G_m\right)\right\rangle\!\!\right\rangle = \frac{(2\pi)^2}{v\,s^2\sqrt{5}}\langle \mathrm{Tr}[\boldsymbol{Q}(\boldsymbol{x})^2]\rangle. \tag{30}$$

Although correlation functions (20)–(24) are easily accessible, e.g., in computer simulations, we are not aware of any systematic studies of their properties for chiral liquids. In particular, irreducible parts $G_R^{(1)}$ and $G_R^{(3)}$ being proportional to chirality κ could be used to introduce a measure of phase chirality.

IV. MODEL CALCULATIONS

We closely follow the theory exposed in our previous publications [1,2]. However, because the order parameter components are coupled in the isotropic–BPIII pretransitional region, we include all five helicity modes into the theoretical scheme and carry out the analysis to leading order of the cumulant expansion. The importance of the mode-mode coupling will clearly be demonstrated. We start by noting that the free energy (4) has an upper bound given by the Bogoliubov-Hellman-Feynman inequality [12]

$$F \leqslant F_{trial} = F_0 + \langle H - H_0\rangle_0, \tag{31}$$

where F_0 is calculated from Eq. (4) with the trial Hamiltonian H_0 as well as the average $\langle H-H_0\rangle_0$. One can prove the inequality (31) with the cumulant expansion up to second order. The inequality becomes an equality for $H_0 = H$. It is important to note that the choice of the trial Hamiltonian H_0 is determined by the possibility of evaluating the path integral (11) exactly. Any adjustable parameters introduced in H_0 are best chosen so as to minimize the right-hand side (RHS) of the inequality (31). In order to carry out perturbational calculations, we choose an effective quadratic Hamiltonian depending on five variational parameters Δ_m:

$$H_0/v = \frac{1}{4}\sum_{m,k}\{\Delta_m + [f(m,k)]^2\}|\mu_m(k)|^2, \tag{32}$$

where the chosen form resembles the structure of the quadratic part of $\mathcal{H}$, Eq. (10),

$$\mathcal{H}_2/v = \frac{1}{4}\sum_{m,k}\{\tau_m + [f(m,k)]^2\}|\mu_m(k)|^2. \tag{33}$$

Here,

$$f(m,k) = \left(\frac{\kappa m}{2\sqrt{\rho_m}} - k\sqrt{\rho_m}\right) \tag{34}$$

and

$$\tau_m = t - \frac{\kappa^2 m^2}{4\rho_m}, \quad \rho_m = 1 + \frac{1}{6}\rho(4-m^2). \tag{35}$$

Equation (32) is a direct generalization of Eq. (10) in Ref. [2]. With the trial Hamiltonian (32), the calculation of the RHS of Eq. (31) is carried out in a similar fashion as in Refs. [1,2]. One finds

$$-\mathcal{T}^{-1}F_0 = \ln Z_0 = \sum_{\substack{m,\boldsymbol{k}\\ k<\Lambda}}\frac{1}{2}\ln\frac{2\mathcal{T}}{\Delta_m + [f(m,k)]^2} \tag{36}$$

and

$$\langle H - H_0\rangle_0 = \sum_m\left\{\tau_m - \Delta_m + \frac{14}{15}\sum_{m'} S_{m'}(\Delta_{m'})\right\}S_m(\Delta_m), \tag{37}$$

where

$$S_m(\Delta_m) = \frac{1}{4}\sum_k\langle|\mu_m(k)|^2\rangle_{H_0} = \frac{\mathcal{T}}{4\pi^2}\int_0^\Lambda\frac{k^2 dk}{\Delta_m + [f(m,k)]^2}. \tag{38}$$

Therefore, we can improve the previous approach [2] by minimizing the (dimensionless) trial free energy F_{trial}

$=-\mathcal{T}\ln Z_0+\langle H-H_0\rangle_0$ with respect to the five variational parameters Δ_m for fixed relative temperature t, energy scale of the fluctuations $\mathcal{T}$, relative elastic constant ρ, and cutoff $\Lambda=n\kappa$ with n varying from 1 to 4 [2]. The $\Delta_m^{-1/2}$ parameters are the correlation lengths and $S_m(\Delta_m)$ is the self-energy function associated with the mode m. As already mentioned before, the cutoff parameter Λ has to be introduced to eliminate modes that are not described by the mesoscopic Hamiltonian. But, as we will show, in a reasonable range for the cutoff radius, the calculations yield qualitatively similar results and quantities, such as $G^{(1)}, G^{(3)}$ or the optical activity, are practically independent of the cutoff for $\Lambda \gtrsim 3$. The dimensionless absolute temperature $\mathcal{T}$ is close to the clearing point temperature, but we find it more convenient to introduce the parameter $\alpha=\mathcal{T}/(60\pi^2)$ used in previous publications [1,2]. A thorough discussion of all parameters except ρ, which is not present for $m=2$ mode, is found in Ref. [2]. As concerning ρ, it is estimated with the help of the results given in Ref. [13]. By employing the transformation from the tensorial to the director picture, we find that $\rho=6k_{11}/(3k_{22}-k_{11}+k_{33})$, where k_{ii} are the Oseen-Zoher-Frank elastic constants. Choosing typical values for k_{ii} in the nematic phase [14], we obtain $\rho\approx 2.8$. On the other hand, close to the nematic-isotropic phase transition, these can all be taken equal yielding $\rho\approx 2$. Estimates of Stinson and Litster show that $\rho\approx 1$ for MBBA [15]. Our analysis will be carried out for ρ between 0 and 3. We show that the parameter ρ is of secondary importance for the isotropic liquid.

In order to obtain the equilibrium free energy, and hence also the thermodynamic functions of interest, the trial free energy has to be minimized with respect to the variational parameters Δ_m. It leads to nonlinear equations

$$\left[\tau_p-\Delta_p+\frac{28}{15}\sum_m S_m(\Delta_m)\right]\frac{\partial S_p}{\partial \Delta_p}=0. \tag{39}$$

Differentiating Eq. (38) with respect to Δ_p, one finds that $\partial S_p/\partial\Delta_p<0$ implying that Eq. (39) becomes reduced to a set of five self-consistent equations:

$$\Delta_p=\tau_p+\frac{28}{15}\sum_m S_m(\Delta_m). \tag{40}$$

By substituting $\Delta_p=\Delta+\tau_p$, these are simplified to one equation as

$$\Delta=\frac{28}{15}\sum_m S_m(\Delta+\tau_m)>0. \tag{41}$$

Such a simple reduction exists only in the lowest-order cumulant expansion. We find that $\Delta_m=\Delta_{-m}$. Additionally, within the stability limit of the Hamiltonian (1), the dominant correlation length corresponds to the $m=\pm 2$ modes. The smallest correlation length is associated with the mode $m=0$. Also note that in the absence of fourth-rank terms in the Hamiltonian the theory reduces to standard Gaussian correlations with $\Delta_m=\tau_m$.

A numerical analysis of the model requires stability of the Gaussian trial Hamiltonian (32). This is guaranteed given that solutions for Δ_m satisfy $\Delta_m>0$ ($m=-2,\ldots,2$). Under these circumstances, the liquid state is at least a metastable one. We cannot prove, however, that the isotropic liquid is absolutely stable for all cases with $\Delta_m>0$. Most probably, there exists a region in the parameter space where the cholesteric phase or cubic blue phases take over, but inclusion of all these phases into the perturbational scheme introduced here is quite difficult and has not been done as yet.

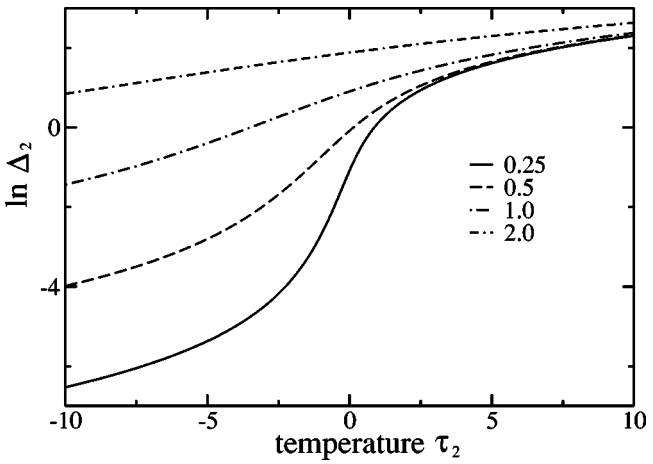

FIG. 1. Dependence of the variational parameter $\Delta_2=\Delta+\tau_2$ on the relative temperature τ_2 for $\alpha=0.2$, $n=1$, $\rho=0$, and for κ varying between 0.25 and 2.0. Curves are parametrized by chirality κ.

Typical numerical solutions for Δ are shown in Fig. 1. These look qualitatively similar to those obtained in Ref. [2]. However, a closer inspection of the figure in the vicinity of $\tau_2\approx 0$ shows the differences. This is best illustrated in Fig. 2, where Δ_2 calculated with five modes is compared with the case where only the $m=2$ mode was retained [2]. We note that both theories give similar results at high temperatures and/or high chiralities. However, these differ significantly for $\tau_2\approx 0$, where a qualitative change of the correlations takes place. We find that the extra modes couple with each other,

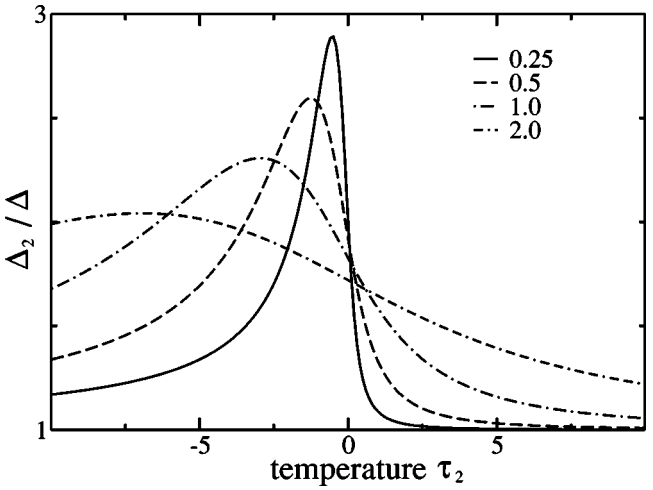

FIG. 2. Temperature variation of Δ_2/Δ, where Δ is taken from Ref. [2]. Calculations are carried out for $\alpha=0.2$, $n=1$, $\rho=0$, and for κ varying from 0.25 to 2. The curves are parametrized by chirality κ.

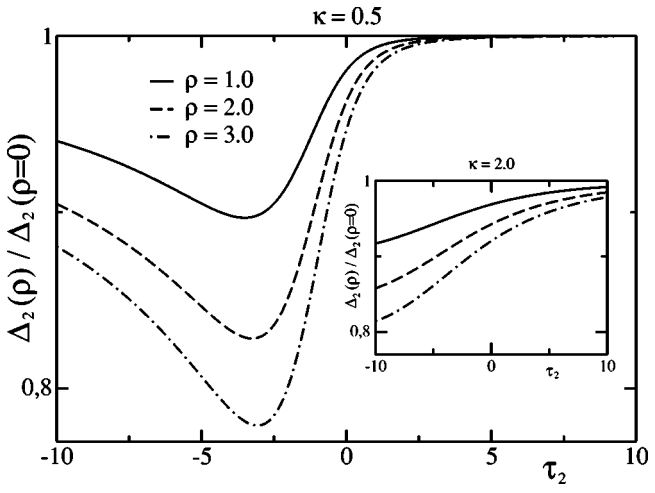

FIG. 3. Temperature variation of $\Delta(\rho)/\Delta(\rho=0)$. Calculations are carried out for $\alpha=0.2$, $n=1$, and for $\kappa=0.5{,}2$ (inset).

thus enhancing correlations in this regime, which is in line with experiments in the vicinity of BPIII–isotropic phase transition (see, e.g., Ref. [7]). A similar behavior is observed close to the isotropic-cholesteric phase transition as will be discussed in our forthcoming publication [16]. Also please note that the relative elastic constant ρ is of secondary importance for the properties of high-temperature phase ($\tau_2>0$), as illustrated in Fig. 3.

Finally, we comment on the possibility of a phase transition between BPIII and the high-temperature isotropic liquid. Unfortunately, such a phase transition is not realized in the lowest-order cumulant expansion calculations. This is recognized on the relationship between τ_p and Δ_l:

$$\frac{\partial\tau_p}{\partial\Delta_l}=\delta_{pl}-\frac{28}{15}\frac{\partial S_l(\Delta_l)}{\partial\Delta_l}>0, \tag{42}$$

which means that a critical point ($\partial\tau_p/\partial\Delta_l=0$) and a first-order phase transition ($\partial\tau_p/\partial\Delta_l<0$) are not present in our theory. It would require to take into account higher orders of the cumulant expansion as demonstrated in Ref. [2]. However, as we show, by studying the correlation functions, the specific heat, and the pretransitional optical activity, the existence of the two differently correlated regions in the thermodynamic space is evident even in this order of calculations. The results are presented on two plots for each case. One for cutoff parameter $n=1$ and the other for $n=3$. The different lines on each plots correspond to different values of the chirality changing from $\kappa=0.2$ to $\kappa=3$, but many quantities of interest are practically cutoff independent for $\kappa\gtrsim 3$.

After introducing the perturbational scheme, we use it to discuss the correlation functions $G^{(L)}$, the optical activity tensor, and the specific heat. Also, we calculate the averaged value of the chiral invariant in Eq. (2), previously used to discuss ordering in chiral isotropic liquids [8,19].

A. Correlation functions

We assume that the correlation functions G_m are Lorentzian-like with

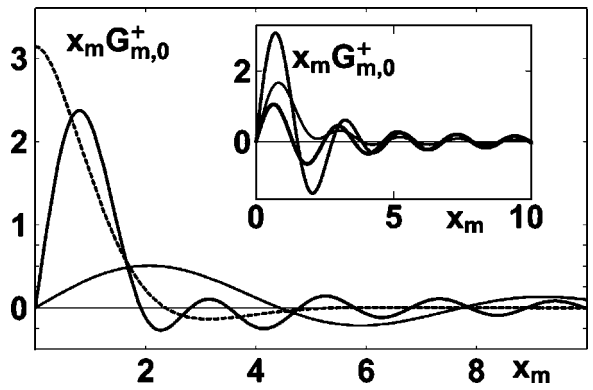

FIG. 4. Dependence of correlation mode $G^{+}_{m,0}$ multiplied by the relative reduced distance x_m on x_m. Curves are parametrized by $\Lambda_m=1{,}3{,}\infty$ and $q_m=1$. The inset shows $G^{+}_{m,0}$ for $q_m=0{,}2{,}4$ and $\Lambda_m=3$. Thicker lines correspond to larger values of the parameters. The limiting curve, $\Lambda_m=\infty$, $q_m=1$, is shown as dashed line.

$$G_m=\frac{g_m}{\xi_m^{-2}+(k-k_m)^2}, \tag{43}$$

where $g_m=g_{-m}$ and $k_m=-k_{-m}$. The model calculations of the preceding section, Eqs. (31)–(41), are special cases of Eq. (43) with

$$\xi_m^{-2}=\frac{\Delta_m}{\rho_m},\quad \rho_m=1+\frac{1}{6}\rho(4-m^2),\quad g_m=\frac{2\mathcal{T}}{\rho_m},\quad k_m=\frac{\kappa m}{2\rho_m}. \tag{44}$$

Also, the ordinary Gaussian theory is recovered from Eq. (43) if we take $\Delta_m=\tau_m$.

Substitution of Eq. (43) into Eqs. (20)–(24) yields the formulas for the correlation modes $G^{(L)}$, $L=0,\ldots 4$, which are linear combinations of m-(anti) symmetrized averages $G^{\pm}_{m,n}$:

$$G^{\pm}_{m,n}=\int_0^{\Lambda_m}q^2\left[\frac{1}{1+(q-q_m)^2}\pm\frac{1}{1+(q+q_m)^2}\right]u_n(q\,x_m)\,dq$$
$$=\frac{\xi_m}{g_m}\langle\!\langle (G_m\pm G_{-m})\,u_n\rangle\!\rangle,\ m\geqslant 0. \tag{45}$$

Here, the model parameters are measured relative to the dimensionless correlation length ξ_m: $x_m=|\boldsymbol{x}-\boldsymbol{x}'|/\xi_m$, $q_m=k_m\xi_m$, $\Lambda_m=\Lambda\xi_m$. The functions $G^{\pm}_{m,n}$ could be expressed in terms of sine (Si) and cosine (Ci) integral functions but, as the formulas are lengthy, we do not present them explicitly here. Instead, a typical behavior of $G^{\pm}_{m,n}$ on the relative, reduced distance x_m is shown in Figs. 4–7.

We observe that the real space behavior of $G^{\pm}_{m,n}$ splits into three classes represented by (a) $G^{+}_{m,0}$, (b) $G^{+}_{m,2}$, $G^{+}_{m,4}$, and (c) $G^{-}_{m,1}$, $G^{-}_{m,3}$ ($m\neq 0$) functions. A major difference between them is their cutoff dependence, which can be studied by analyzing the limit $\Lambda_m\to\infty$. More specifically, it is found that only the functions belonging to the classes (a) and (b)

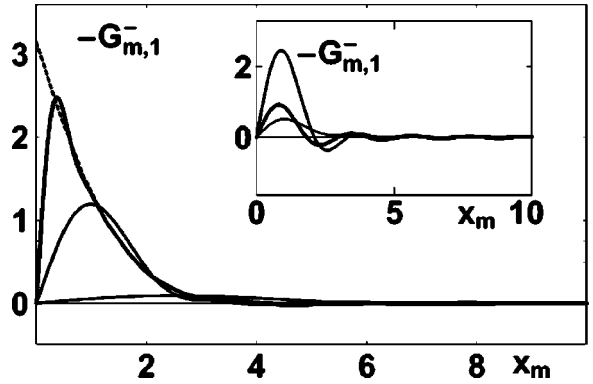

FIG. 5. Dependence of correlation mode $-G^{-}_{m,1}$ on the relative reduced distance x_m. The curves are parametrized by $\Lambda_m = 1,3,10,\infty$ and $q_m = 1$. The inset shows $-G^{-}_{m,1}$ for $q_m = 0.5,2,4$ and $\Lambda_m = 3$. Thicker lines correspond to larger values of the parameters. The limiting curve, $\Lambda_m = \infty$, $q_m = 1$, is shown as dashed line.

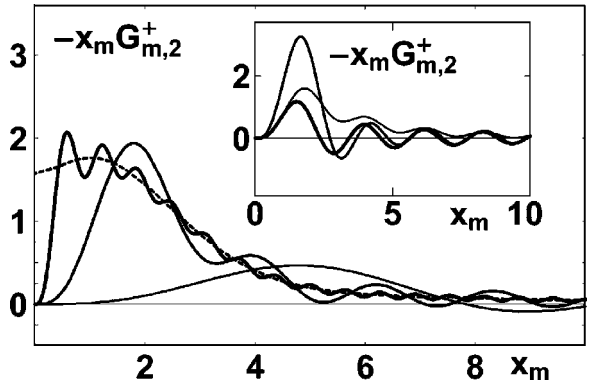

FIG. 6. Dependence of correlation mode $-x_m G^{+}_{m,2}$ on the relative reduced distance x_m. Curves are parametrized by $\Lambda_m = 1,3,10,\infty$ and $q_m = 1$. The inset shows $-x_m G^{+}_{m,2}$ for $q_m = 0.5,2,4$ and $\Lambda_m = 3$. Thicker lines correspond to larger values of the parameters. The limiting curve, $\Lambda_m = \infty$, $q_m = 1$, is shown as dashed line.

show, for small x_m, strong dependence on the cutoff. In particular, $G^{+}_{m,0}$ [see Fig. (4)] diverges linearly with Λ_m as x_m tends to zero:

$$\lim_{\Lambda_m \to \infty} G^{+}_{m,0} = \frac{\pi e^{-x_m}[\cos(q_m x_m) + q_m \sin(q_m x_m)]}{x_m}. \tag{46}$$

All remaining functions of classes (b) and (c) disappear by symmetry when x_m tends to 0 and Λ_m is finite. As high momenta are important for small values of x_m, we expect that overall cutoff dependence of the functions (b) and (c) should be of secondary importance. Indeed, this is the case for the class (c), Figs. 5 and 7, where contributions of the high energy modes (large k vectors) partly cancel out due to $G_m - G_{-m}$ dependence under the integral (45). But, as the limits $x_m \to 0$ and $\Lambda_m \to \infty$ do not commute, a cutoff dependence could also be observed for a small x_m. To be more specific, let us concentrate on the parameter dependence of $G^{-}_{m,1}$ function in a more detailed way. We find that the first peak of $G^{-}_{m,1}$, being located at $x^{*}_m \approx 4.49/\Lambda_m$ ($\Lambda_m \gtrsim 3$), results from a combination of chiral interactions and high energy modes. For $x_m > x^{*}_m$, the functions $G^{-}_{m,1}$ could be replaced by their $\Lambda_m \to \infty$ counterparts and these fall off to zero for $x_m \to 0$ ($x_m < x^{*}_m$). When $\Lambda_m \to \infty$, we find

$$\lim_{\Lambda_m \to \infty} G^{-}_{m,1} = -\frac{\pi e^{-x_m}[(1 + x_m)\sin(x_m q_m) - x_m q_m \cos(x_m q_m)]}{x_m^2}, \tag{47}$$

where the peak at x^{*}_m for finite Λ yields a nonzero value of $G^{-}_{m,1}$ at $x_m = 0$ for the limiting case (47). A similar behavior is observed for $G^{-}_{m,3}$, as shown in Fig. 7. Note again that both $G^{-}_{m,1}$ and $G^{-}_{m,3}$ vanish with vanishing chirality, with the leading term being proportional to q_m.

Functions $G^{+}_{m,2}$ and $G^{+}_{m,4}$ look similar to $G^{+}_{m,0}$ except that these vanish for $x_m = 0$ and finite Λ_m. A first peak of $G^{+}_{m,2}$ and $G^{+}_{m,4}$, being located at $x^{*}_m \sim 1/\Lambda_m$, is due to high-energy modes and diverges linearly with Λ_m. Again the limiting cases could easily be found. For example,

$$\lim_{\Lambda_m \to \infty} G^{+}_{m,2} = \frac{\pi\{-3 + e^{-x_m}[3 + (1 + q_m^2)x_m(3 + x_m)]\cos(q_m x_m)\}}{(1 + q_m^2)x_m^3} - \frac{\pi e^{-x_m} q_m [3 - (1 + q_m^2)x_m^2]\sin(q_m x_m)}{(1 + q_m^2)x_m^3}. \tag{48}$$

Note that the formulas derived here are independent of the details of a model used to calculate Δ_m.

Now, by taking appropriate linear combinations of $G^{\pm}_{m,n}$ functions [see, Eqs. (20)–(24) and (45)], the properties of $G^{(L)}$s could easily be studied for the model (31) and (32). In particular, we find that the temperature dependence of $G^{(L)}$s provides a clear distinction between the two differently correlated regions in the thermodynamic space as at low temperatures the correlation modes are much stronger than those at high temperatures. The purely chiral functions $G^{(1)}_R$ and $G^{(3)}_R$ are found weakly dependent on the cutoff for distances above the first peak. The dominant contributions come from fluctuations on the sphere of k vectors, where $f(m,k)^2$, Eq. (34), is minimal, that is, for $k \approx \kappa$. These fluctuations are induced by the presence of chiral interactions and their contribution, measured by $G^{(1)}_R$ and $G^{(3)}_R$, disappears for nonchiral systems. In this sense, $G^{(1)}_R$ (or functions involving $G^{(1)}_R$) could serve as a measure of phase chirality. Further-

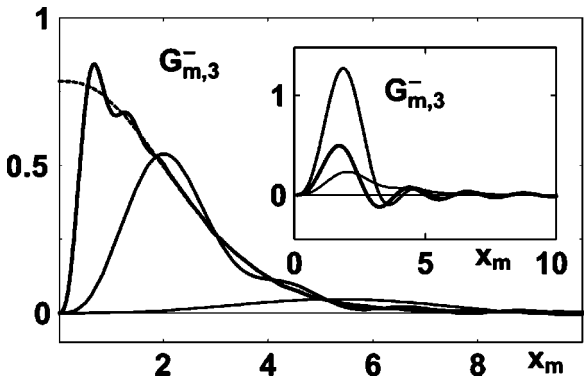

FIG. 7. Dependence of correlation mode $G^-_{m,3}$ on relative reduced distance x_m. Curves are parametrized by $\Lambda_m=1,3,10,\infty$ and $q_m=1$. The inset shows $G^-_{m,3}$ for $q_m=0.5,2,4$ and $\Lambda_m=3$. Thicker lines correspond to larger values of the parameters. The limiting curve, $\Lambda_m=\infty$, $q_m=1$, is shown as dashed line.

more, the position of the first peak could be used to specify the distance above which chirality-induced modes dominate.

Finally, we note that the effect of the parameter ρ ($\rho>0$) on the correlations is to introduce weights for linear combinations of $G^{\pm}_{m,n}$ entering $G^{(L)}$ and to rescale correlation lengths. As this rescaling goes through ρ_m, the effect is weak for experimentally accessible values of this parameter. The only qualitatively different case is that of $\rho=0$ ($\rho_m=1$). For $\rho=0$, the contribution to G^2 and G^4 of high-energy modes largely cancels out due to subtractions of different $G^+_{m,n}$ functions [see Eqs. (22) and (24)].

B. Pretransitional optical activity

The explicit form of the pair correlation function (either in Fourier or in real space) is a different step towards calculations of experimentally accessible quantities, such as intensity of scattered light or optical activity. We concentrate here on the optical activity in the isotropic phase.

The optical-activity tensor of an isotropic fluid, $\gamma_{ijk}=\epsilon_{ijk}\gamma$, measures, according to Landau [17], the dependence of the dielectric tensor on the variation of the local electric field. The corresponding expressions for cholesterics and blue phases have been discussed by Bensimon *et al.* [18]. They calculated the leading term to γ_{ijk} assuming that the maximal correlation length of $\boldsymbol{G}$ is negligible compared to the wavelength of the incident light. Their formula has subsequently been generalized by Lubensky and Stark [8] to the case when the isotropic fluid is close in temperature to the cholesteric or blue phase. Following the derivation given in Refs. [18,8] one finds that

$$\gamma=\frac{s^2\epsilon_{\alpha\delta\mu}}{12\pi\epsilon_0\xi_R^2}\int d^3\boldsymbol{x}G_{\alpha\beta\gamma\delta}(x)x_\mu(\partial_\beta\partial_\gamma-q^2\delta_{\beta\gamma})\left[\frac{e^{-i\boldsymbol{q}\cdot\boldsymbol{x}}}{x}\right]$$

$$=\frac{s^2}{\pi^2\epsilon_0\xi_R^2}(\gamma_0+\gamma_2k_0^2+\cdots), \tag{49}$$

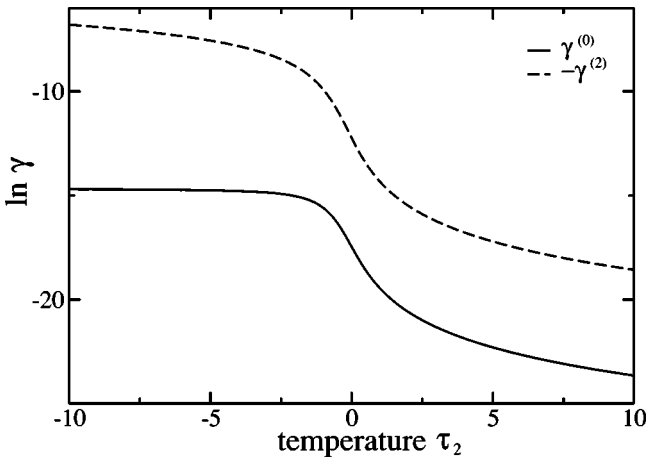

FIG. 8. Dependence of optical activity coefficients γ_0 and γ_2 on temperature τ_2. The solid line corresponds to γ_0, whereas the dashed line describes $-\gamma_2$. Parameters used are $\alpha=0.2$, $\rho=1$, $\kappa=0.25$, and $n=1$.

$$\gamma_0=\frac{1}{12}\int_0^\Lambda dqq[G_1(q)-G_{-1}(q)]\overset{\Lambda\to\infty}{\to}\frac{\mathcal{T}\kappa\pi}{12\left(1+\frac{1}{2}\rho\right)^{5/4}\sqrt{\Delta_1}}, \tag{50}$$

$$\gamma_2=-\frac{1}{18}\int_0^\Lambda dq\frac{1}{q}[G_1(q)-G_{-1}(q)]-\frac{2}{9}\int_0^\Lambda dq\frac{1}{q}\times[G_2(q)-G_{-2}(q)]$$

$$\overset{\Lambda\to\infty}{\to}-\frac{2\mathcal{T}\kappa\pi}{9}\left[\frac{2}{\sqrt{\Delta_2}(\Delta_2+\kappa^2)}+\frac{1+\frac{1}{2}\rho}{\left(1+\frac{1}{2}\rho\right)^{1/4}\sqrt{\Delta_1}\left[4\left(1+\frac{1}{2}\rho\right)^{1/2}\Delta_1+\kappa^2\right]}\right]. \tag{51}$$

Here, ϵ_0 is the average dielectric constant of the system and k is the wave vector of the incident light in units of ξ_R^{-1}. Note that in Eq. (49) not only modes with $m=\pm1$ are present but also those with $m=\pm2$, in agreement with experiments by Battle *et. al.* [4] and Ennis *et al.* [3]. The angle of rotation of the light is given by $\phi=(k_0^2/2)\gamma$. Also, please observe ρ dependence of γ.

Does the optical activity change sign, as observed experimentally? The optical activity depends on the product of chirality and correlation length. For relatively low chiralities, there are long-range correlations in the BPIII phase. Because small changes in κ cause a big difference of Δ, $\gamma\approx\xi$ is

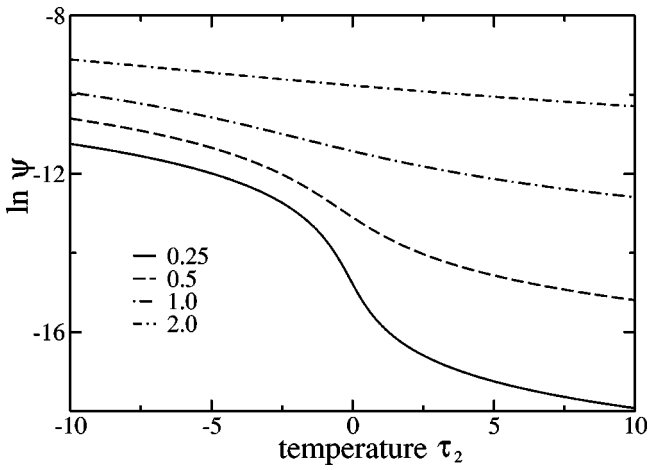

FIG. 9. Dependence of order parameter ψ on temperature τ_2. Due to a negative value of ψ, the plot shows its absolute value τ_2. Parameters used are $\alpha=0.2$, $\rho=1$, and $n=1$. Chirality κ varies from 0.25 to 2.

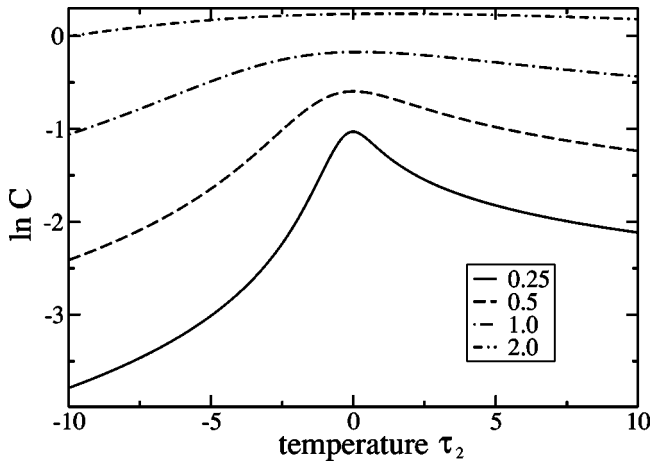

FIG. 10. Dependence of specific heat on temperature τ_2 for $\alpha=0.2$, $\rho=1$, $\kappa=0.25$, and for $n=1$.

valid. This picture turns over where chiralities are large enough. In this situation, $\gamma\approx\kappa$. Additionally, due to second-order term in Eq. (49), optical activity can change sign for large enough value of k_0. A model calculation of the first two terms of total optical activity is shown in Fig. 8.

C. Order parameter $\langle\int d^3r\,\epsilon_{ijk}Q_{il}\partial_j Q_{kl}\rangle$

Another quantity, which could give a clear distinction between the isotropic phases of chiral liquid crystals is the (dimensionless) order parameter $\psi=\xi_R/s^2\langle(\nabla\times\mathbf{Q})\cdot\mathbf{Q}\rangle$ introduced in Refs. [19,8]. Its definition shows that it measures local twisting power

$$\begin{aligned}\psi&=\sum_{k,m} m\,kG_m(k)\\&=4\pi\kappa\mathcal{T}\Bigg\{\left[16+\frac{4}{\left(1+\frac{1}{2}\rho\right)^2}\right]\Lambda\\&\quad+2\pi\left(-6\sqrt{\Delta_2}+\frac{2\kappa^2}{\sqrt{\Delta_2}}\right)+\frac{\pi}{\left(1+\frac{1}{2}\rho\right)^3}\\&\quad\times\left[-3\left(1+\frac{1}{2}\rho\right)^{1/4}\sqrt{\Delta_1}+\frac{\kappa^2}{4\left(1+\frac{1}{2}\rho\right)^{1/4}\sqrt{\Delta_1}}\right]\\&\quad+O'\left(\frac{1}{\Lambda}\right)\Bigg\}.\end{aligned}\tag{52}$$

Dependence of ψ on the temperature τ_2 is shown in Fig. 9. Note that ψ behaves in a similar way as the correlation length. More specifically, there are two regimes characterized by small and large values of this parameter, but, as already discussed before, no phase transition between both regimes is predicted by the theory. Note that the term proportional to Λ does not depend on τ_2.

D. Specific heat

The relatively simple form of the effective Hamiltonian H' allows us to calculate practically all experimentally accessible quantities. We illustrate this further by calculating the specific heat of the chiral isotropic liquid. For our case, it reads

$$C=-\mathcal{T}\frac{\partial^2(F/v)}{\partial\mathcal{T}^2}\approx\mathcal{T}\sum_m\frac{\partial\Delta_m}{\partial\tau}\frac{\partial S_m}{\partial\Delta_m},\tag{53}$$

and does not show a singularity. However, there exists a clear maximum in the specific heat for $\tau_2\approx0$ and at moderate chiralities, Fig. 10, supporting previous observations that the structure of short-range correlations changes in this regime. The effect almost disappears for $\kappa>1$. Though the model does not display a singularity or a discontinuity characteristic of a phase transition, the behavior is typical of a pretransitional regime where enhance of correlations is indicative of a nearby critical point. Such a critical point can be accounted for by the third-order cumulant expansion, as shown with the help of calculations with a scalar order parameter [1,2].

V. SUMMARY

We have presented a systematic approach to study the effect of correlations between the fluctuating helicity modes of the alignment tensor in the isotropic phases of chiral liquid crystals. One of the main advantages of the present approach is that it treats the fluctuations of the various modes on an equal footing and thus it allows one to compare their relative importance. The only other calculations in this direction we are aware of are those for nematic liquid crystals by Priest and Lubensky [20] and by Wang and Keyes [21]. More recently, some aspects of tensor fluctuations were also con-

sidered for spontaneously ordered chiral phases, relevant to bent-core liquid crystals [22].

Here, the exact representation of the real-space two-point correlation function has been derived to show that the irreducible parts $G_R^{(1)}$ and $G_R^{(3)}$ of **G** can be used to characterize phase chirality of an isotropic liquid. These quantities, especially $G_R^{(1)}$, seem more adequate for that than, e.g., optical activity. The reason is that the leading term of the optical activity depends upon secondary $m=\pm 1$ modes, while the most important for chiral liquids are $m=\pm 2$ modes. Terms that enter $G_R^{(1)}$ contribute to the intensity of light scattered at wave vector q and could, at least, in principle, be extracted by incorporating appropriate polarization vectors for the incident and the scattered lights. Also please note that nonzero values of $G_R^{(1)}$ and $G_R^{(3)}$ indicate that chirality induces local polar ordering even in the absence of dipole moments. Both functions vanish for nonchiral and nonpolar liquids and could easily be determined, e.g., from computer simulations on molecular models. Although this has not been done so far, such simulations would be of interest as these could provide a connection between microscopic modeling and phenomenological approach.

The theory has been illustrated with calculations that are complete up to the first-order cumulant expansion. The calculated quantities such as the correlation lengths and the correlation functions of the tensor order parameter, the optical activity, the chiral order parameter ψ, and the specific heat show two distinct isotropic regimes. The first one is highly correlated and appears at low chirality and/or temperature and differs from a weakly correlated one that is stable at $\tau_2 > 0$. Furthermore, we proved that the $m \neq 2$ modes are of secondary importance except close to $\tau_2 \approx 0$, where the two-point correlations change their character. In this regime, which could be considered as a sign of a pretransitional BPIII–isotropic regime, the correlations between the components of the tensor order parameter are important, in agreement with experiment. However, the lowest-order cumulant expansion cannot account for a ''sharp'' phase transition between the high-temperature isotropic liquid and the BPIII, even with all five modes included. Thus going beyond the leading order seems essential.

Indeed, as we showed in our previous publications [1,2], the third-order cumulant expansion with a simplified Gaussian trial Hamiltonian allows one to recover a true phase transition between the isotropic phases within the Landau–Ginzburg–de Gennes Hamiltonian. Though, as we believe, such calculations with the exact Hamiltonian are relevant to obtain a fully consistent picture of the chiral isotropic phases, many of the results presented here are expected to remain unaffected. One of them is the detailed analysis of the correlations as given in Secs. II, III, and IV c and presented in Figs. 4–7. Clearly, these are independent of detailed models used to calculate Δ_m. The model should also be correct at least in the high-temperature isotropic regime where it becomes convergent to the previously studied, simplified case [1,2]. Finally, the improved calculations cannot remove correlations predicted by the first-order analysis and the true phase transition of such an improved analysis would be expected for $\tau_2 \approx 0$ (see, Figs. 1,2 and 10). This expectation is supported by Fig. 5 of Ref. [1] and Fig. 11 of Ref. [2], where the phase transition of the simplified model is also observed for $\tau_2 \approx 0$.

One of the new features of higher-order calculations could be a momentum dependence of Δ_m parameters, which would replace nonlinear equations (40) by integral equations. Experiments by Koistinen and Keyes [7] seem to indicate that G_m may indeed be more complicated function than a simple Lorentzian.

ACKNOWLEDGMENTS

This work was supported by the Polish Project (KBN) No. 5 P03B 052 20 and by the project C12 of Collaborative Research Center 382 of the Deutsche Forschungsgemeinschaft (DFG).

APPENDIX: UNIAXIAL BASIS TENSORS

We list below:

$$\boldsymbol{M}_0^{(0)} = \frac{1}{6\sqrt{5}}\{6\,(\hat{\boldsymbol{x}}\otimes\hat{\boldsymbol{x}}\otimes\hat{\boldsymbol{x}}\otimes\hat{\boldsymbol{x}}+\hat{\boldsymbol{y}}\otimes\hat{\boldsymbol{y}}\otimes\hat{\boldsymbol{y}}\otimes\hat{\boldsymbol{y}}+\hat{\boldsymbol{z}}\otimes\hat{\boldsymbol{z}}\otimes\hat{\boldsymbol{z}}\otimes\hat{\boldsymbol{z}}) - 2\,(\hat{\boldsymbol{x}}\otimes\hat{\boldsymbol{x}}+\hat{\boldsymbol{y}}\otimes\hat{\boldsymbol{y}}+\hat{\boldsymbol{z}}\otimes\hat{\boldsymbol{z}})\otimes(\hat{\boldsymbol{x}}\otimes\hat{\boldsymbol{x}}+\hat{\boldsymbol{y}}\otimes\hat{\boldsymbol{y}}+\hat{\boldsymbol{z}}\otimes\hat{\boldsymbol{z}}) + 3[(\hat{\boldsymbol{x}}\otimes\hat{\boldsymbol{y}}+\hat{\boldsymbol{y}}\otimes\hat{\boldsymbol{x}})\otimes(\hat{\boldsymbol{x}}\otimes\hat{\boldsymbol{y}}+\hat{\boldsymbol{y}}\otimes\hat{\boldsymbol{x}}) + (\hat{\boldsymbol{x}}\otimes\hat{\boldsymbol{z}}+\hat{\boldsymbol{z}}\otimes\hat{\boldsymbol{x}})\otimes(\hat{\boldsymbol{x}}\otimes\hat{\boldsymbol{z}}+\hat{\boldsymbol{z}}\otimes\hat{\boldsymbol{x}}) + (\hat{\boldsymbol{y}}\otimes\hat{\boldsymbol{z}}+\hat{\boldsymbol{z}}\otimes\hat{\boldsymbol{y}})\otimes(\hat{\boldsymbol{y}}\otimes\hat{\boldsymbol{z}}+\hat{\boldsymbol{z}}\otimes\hat{\boldsymbol{y}})]\}, \tag{A1}$$

$$\boldsymbol{M}_0^{(1)} = \frac{-i}{2\sqrt{10}}[2(\hat{\boldsymbol{x}}\otimes\hat{\boldsymbol{x}}-\hat{\boldsymbol{y}}\otimes\hat{\boldsymbol{y}})\otimes(\hat{\boldsymbol{x}}\otimes\hat{\boldsymbol{y}}+\hat{\boldsymbol{y}}\otimes\hat{\boldsymbol{x}}) - 2(\hat{\boldsymbol{x}}\otimes\hat{\boldsymbol{y}}+\hat{\boldsymbol{y}}\otimes\hat{\boldsymbol{x}})\otimes(\hat{\boldsymbol{x}}\otimes\hat{\boldsymbol{x}}-\hat{\boldsymbol{y}}\otimes\hat{\boldsymbol{y}}) + (\hat{\boldsymbol{x}}\otimes\hat{\boldsymbol{z}}+\hat{\boldsymbol{z}}\otimes\hat{\boldsymbol{x}})\otimes(\hat{\boldsymbol{y}}\otimes\hat{\boldsymbol{z}}+\hat{\boldsymbol{z}}\otimes\hat{\boldsymbol{y}}) - (\hat{\boldsymbol{y}}\otimes\hat{\boldsymbol{z}}+\hat{\boldsymbol{z}}\otimes\hat{\boldsymbol{y}})\otimes(\hat{\boldsymbol{x}}\otimes\hat{\boldsymbol{z}}+\hat{\boldsymbol{z}}\otimes\hat{\boldsymbol{x}})], \tag{A2}$$

$$\boldsymbol{M}_0^{(2)} = \frac{1}{6\sqrt{14}}[4\hat{\boldsymbol{x}}\otimes\hat{\boldsymbol{x}}\otimes(\hat{\boldsymbol{x}}\otimes\hat{\boldsymbol{x}}-2\hat{\boldsymbol{y}}\otimes\hat{\boldsymbol{y}}+\hat{\boldsymbol{z}}\otimes\hat{\boldsymbol{z}}) + 4\hat{\boldsymbol{z}}\otimes\hat{\boldsymbol{z}}\otimes(\hat{\boldsymbol{x}}\otimes\hat{\boldsymbol{x}}+\hat{\boldsymbol{y}}\otimes\hat{\boldsymbol{y}}-2\,\hat{\boldsymbol{z}}\otimes\hat{\boldsymbol{z}}) + 4\hat{\boldsymbol{y}}\otimes\hat{\boldsymbol{y}}\otimes(\hat{\boldsymbol{y}}\otimes\hat{\boldsymbol{y}}-2\,\hat{\boldsymbol{x}}\otimes\hat{\boldsymbol{x}}+\hat{\boldsymbol{z}}\otimes\hat{\boldsymbol{z}}) + 6(\hat{\boldsymbol{x}}\otimes\hat{\boldsymbol{y}}+\hat{\boldsymbol{y}}\otimes\hat{\boldsymbol{x}})\otimes(\hat{\boldsymbol{x}}\otimes\hat{\boldsymbol{y}}+\hat{\boldsymbol{y}}\otimes\hat{\boldsymbol{x}}) - 3(\hat{\boldsymbol{x}}\otimes\hat{\boldsymbol{z}}+\hat{\boldsymbol{z}}\otimes\hat{\boldsymbol{x}})\otimes(\hat{\boldsymbol{x}}\otimes\hat{\boldsymbol{z}}+\hat{\boldsymbol{z}}\otimes\hat{\boldsymbol{x}}) - 3\,(\hat{\boldsymbol{y}}\otimes\hat{\boldsymbol{z}}+\hat{\boldsymbol{z}}\otimes\hat{\boldsymbol{y}})\otimes(\hat{\boldsymbol{y}}\otimes\hat{\boldsymbol{z}}+\hat{\boldsymbol{z}}\otimes\hat{\boldsymbol{y}})], \tag{A3}$$

$$\boldsymbol{M}_0^{(3)}=\frac{-i}{2\sqrt{10}}[(\hat{\boldsymbol{x}}\otimes\hat{\boldsymbol{x}}-\hat{\boldsymbol{y}}\otimes\hat{\boldsymbol{y}})\otimes(\hat{\boldsymbol{x}}\otimes\hat{\boldsymbol{y}}+\hat{\boldsymbol{y}}\otimes\hat{\boldsymbol{x}})-(\hat{\boldsymbol{x}}\otimes\hat{\boldsymbol{y}}+\hat{\boldsymbol{y}}\otimes\hat{\boldsymbol{x}})\otimes(\hat{\boldsymbol{x}}\otimes\hat{\boldsymbol{x}}-\hat{\boldsymbol{y}}\otimes\hat{\boldsymbol{y}})+2(\hat{\boldsymbol{y}}\otimes\hat{\boldsymbol{z}}+\hat{\boldsymbol{z}}\otimes\hat{\boldsymbol{y}})\otimes(\hat{\boldsymbol{x}}\otimes\hat{\boldsymbol{z}}+\hat{\boldsymbol{z}}\otimes\hat{\boldsymbol{x}})$$
$$-2(\hat{\boldsymbol{x}}\otimes\hat{\boldsymbol{z}}+\hat{\boldsymbol{z}}\otimes\hat{\boldsymbol{x}})\otimes(\hat{\boldsymbol{y}}\otimes\hat{\boldsymbol{z}}+\hat{\boldsymbol{z}}\otimes\hat{\boldsymbol{y}})], \tag{A4}$$

$$\boldsymbol{M}_0^{(4)}=\frac{1}{2\sqrt{70}}[(\hat{\boldsymbol{x}}\otimes\hat{\boldsymbol{x}}+\hat{\boldsymbol{y}}\otimes\hat{\boldsymbol{y}}-4\hat{\boldsymbol{z}}\otimes\hat{\boldsymbol{z}})\otimes(\hat{\boldsymbol{x}}\otimes\hat{\boldsymbol{x}}+\hat{\boldsymbol{y}}\otimes\hat{\boldsymbol{y}}-4\hat{\boldsymbol{z}}\otimes\hat{\boldsymbol{z}})+2\hat{\boldsymbol{x}}\otimes\hat{\boldsymbol{x}}\otimes\hat{\boldsymbol{x}}\otimes\hat{\boldsymbol{x}}+2\hat{\boldsymbol{y}}\otimes\hat{\boldsymbol{y}}\otimes\hat{\boldsymbol{y}}\otimes\hat{\boldsymbol{y}}-8\hat{\boldsymbol{z}}\otimes\hat{\boldsymbol{z}}\otimes\hat{\boldsymbol{z}}\otimes\hat{\boldsymbol{z}}$$
$$+(\hat{\boldsymbol{x}}\otimes\hat{\boldsymbol{y}}+\hat{\boldsymbol{y}}\otimes\hat{\boldsymbol{x}})\otimes(\hat{\boldsymbol{x}}\otimes\hat{\boldsymbol{y}}+\hat{\boldsymbol{y}}\otimes\hat{\boldsymbol{x}})-4(\hat{\boldsymbol{x}}\otimes\hat{\boldsymbol{z}}+\hat{\boldsymbol{z}}\otimes\hat{\boldsymbol{x}})\otimes(\hat{\boldsymbol{x}}\otimes\hat{\boldsymbol{z}}+\hat{\boldsymbol{z}}\otimes\hat{\boldsymbol{x}})-4(\hat{\boldsymbol{y}}\otimes\hat{\boldsymbol{z}}+\hat{\boldsymbol{z}}\otimes\hat{\boldsymbol{y}})\otimes(\hat{\boldsymbol{y}}\otimes\hat{\boldsymbol{z}}+\hat{\boldsymbol{z}}\otimes\hat{\boldsymbol{y}})]. \tag{A5}$$

[1] J. Englert, L. Longa, H. Stark, and H.-R. Trebin, Phys. Rev. Lett. **81**, 1457 (1998).

[2] J. Englert, H. Stark, L. Longa, and H.-R. Trebin, Phys. Rev. E **61**, 2759 (2000).

[3] J. Ennis, J.E. Wyse, and P.J. Collings, Liq. Cryst. **5**, 861 (1981).

[4] P.R. Battle, J.D. Miller, and P.J. Collings, Phys. Rev. A **36**, 369 (1987).

[5] J.E. Wyse, J. Ennis, and P.J. Collings, Phys. Rev. Lett. **62**, 1045 (1989).

[6] B.P. Huff, J.J. Krich, and P.J. Collings, Phys. Rev. E **61**, 5372 (2000).

[7] E.P. Koistinen and P.H. Keyes, Phys. Rev. Lett. **74**, 4460 (1995).

[8] (a) L. Longa and H.-R. Trebin, Phys. Rev. Lett. **71**, 2757 (1993); (b) T.C. Lubensky and H. Stark, Phys. Rev. E **53**, 714 (1996).

[9] H. Grebel, R.M. Hornreich, and S. Shtrikman, Phys. Rev. A **28**, 1114 (1983); **30**, 3264 (1984).

[10] H.G. Kuball, Liq. Cryst. Today **9**, 1 (1999).

[11] See also R. Memmer, J. Chem. Phys. **114**, 8210 (2001).

[12] See, e.g., (a) R.P. Feynman and A.R. Hibbs, *Quantum Mechanics and Path Integrals* (McGraw-Hill, New York, 1965); (b) R.P. Feynman, *Statistical Mechanics* (Benjamin, Reading, MA, 1972); (c) C. Tsallis and L.R. da Silva, Phys. Rev. A **26**, 1095 (1982).

[13] L. Longa, D. Monselesan, and H.R. Trebin, Liq. Cryst. **2**, 769 (1987).

[14] See, e.g., M. Schadt, K. Schmitt, V. Kozinkov, and V. Chigrinov, Jpn. J. Appl. Phys., Part 1 **31**, 2155 (1992).

[15] T.W. Stinson and J.D. Litster, Phys. Rev. Lett. **30**, 688 (1973).

[16] L. Longa and H.-R. Trebin (unpublished).

[17] L.D. Landau and E.M. Lifshitz, *Electrodynamics of Continuous Medium* (Pergamon, Oxford, 1980).

[18] D. Bensimon, E. Domany, and S. Shtrikman, Phys. Rev. A **28**, 427 (1983).

[19] L. Longa, J. Englert, and H.R. Trebin, LMS Symposium on Mathematical Models of Liquid Crystals and Related Polymeric Systems, Durham, 1995 (unpublished).

[20] R.G. Priest and T.C. Lubensky, Phys. Rev. B **13**, 4159 (1976).

[21] Z.H. Wang and P.H. Keyes, Phys. Rev. E **54**, 5249 (1996).

[22] (a) L. Radzihovsky and T.C. Lubensky, Europhys. Lett. **54**, 206 (2001); (b) see also T.C. Lubensky and L. Radzihovsky, Phys. Rev. E **66**, 031704 (2002).